

Magnetic and New Optical Properties in the UV–visible Range of the Egyptian Blue Pigment Cuprorivaite CaCuSi 4 O 10

Laurent Binet, Juliette Lizion, Sylvain Bertaina, Didier Gourier

▶ **To cite this version:**

Laurent Binet, Juliette Lizion, Sylvain Bertaina, Didier Gourier. Magnetic and New Optical Properties in the UV–visible Range of the Egyptian Blue Pigment Cuprorivaite CaCuSi 4 O 10. Journal of Physical Chemistry C, 2021, 125 (45), pp.25189-25196. 10.1021/acs.jpcc.1c06060 . hal-03476635

HAL Id: hal-03476635
https://hal.science/hal-03476635

Submitted on 13 Dec 2021

HAL is a multi-disciplinary open access archive for the deposit and dissemination of scientific research documents, whether they are published or not. The documents may come from teaching and research institutions in France or abroad, or from public or private research centers.

L'archive ouverte pluridisciplinaire **HAL**, est destinée au dépôt et à la diffusion de documents scientifiques de niveau recherche, publiés ou non, émanant des établissements d'enseignement et de recherche français ou étrangers, des laboratoires publics ou privés.

Magnetic And New Optical Properties In The UV-Visible Range Of The Egyptian Blue Pigment Cuprorivaite $CaCuSi_4O_{10}$

Laurent Binet [a*], *Juliette Lizion* [a #], *Sylvain Bertaina* [b] *and Didier Gourier* [a]

[a] *Chimie-ParisTech, PSL University, CNRS, Institut de Recherche de Chimie-Paris, 11 rue Pierre et Marie Curie, 75005 Paris, France*

[b] *Aix-Marseille Université, CNRS, Institut Matériaux, Microélectronique et Nanosciences de Provence, Avenue Escadrille Normandie-Niemen, 13397 Marseille cedex 20, France*

* Email: laurent.binet@chimieparistech.psl.eu

Present Address

Université de Montpellier, Institut Charles Gerhardt Montpellier, CNRS-UM-ENSCM, Place Eugène Bataillon, 34095 Montpellier cedex 5, France

KEYWORDS

Egyptian Blue, Cuprorivaite, Luminescence, Electron Paramagnetic Resonance.

ABSTRACT. Cuprorivaite $CaCuSi_4O_{10}$, the so-called Egyptian blue pigment, exhibits a characteristic and well-known near-infrared luminescence upon excitation in Cu^{2+} *d–d* transitions.

Here we show that upon excitation in the UV, this near-infrared emission is considerably amplified and is accompanied by three different UV-visible emission bands. These four UV-excited emissions are attributed to self-trapped exciton (emission at 2.8 eV), to exciton trapped at Cu site (emission at 1.4 eV) and to trapped exciton emission where the hole only is trapped at Cu site (emissions at 2.65 eV and 3.27 eV). Despite the high Cu content of cuprorivaite, Electron Magnetic Resonance reveals only a weak antiferromagnetic interaction (about 0.08 meV) which averages out the hyperfine interaction of the electron spin with nuclear spins of ^{63}Cu and ^{65}Cu nuclei.

INTRODUCTION

Cuprorivaite $CaCuSi_4O_{10}$ is the major component of the Egyptian Blue pigment,[1,2] the first known synthetic pigment produced by Man. Egyptian Blue has a beautiful color and was used as a substitute for the expensive *Lapis Lazzuli* along the whole Ancient Egypt period until the late Roman time.[3,4] The color of this pigment results from the optical absorption of the Cu^{2+} ions in $CaCuSi_4O_{10}$.[2,5,6] In addition, cuprorivaite exhibits a specific luminescence in the near-infrared (NIR) when excited in the absorption bands of Cu^{2+}.[7,8] This NIR luminescence is related to the deexcitation of Cu^{2+} and is rather uncommon for this ion in an inorganic matrix. Therefore several detailed studies were reported on the optical properties of Cu^{2+} in cuprorivaite but mostly focused on the NIR luminescence.[7-13] Regarding the optical properties of this material in the UV and visible ranges no investigations seem to have been made except an isolated report of a visible cathodoluminescence spectrum.[14] However silicate compounds are well known to exhibit UV-visible luminescence either from self-trapped excitons (STE) or defects.[15,16] Defects in materials are often related to their structure and chemical composition, to the starting materials and the elaboration process. In the field of heritage science determining the history of a material is generally a crucial issue and defects through their optical properties could be highly informative

markers. From a more fundamental perspective, cuprorivaite $CaCuSi_4O_{10}$ can be considered as a 2-dimensional compound with a structure made of double layers of corner-sharing [SiO_4] tetrahedra separated by a layer of Ca^{2+} ions (Fig. 1).

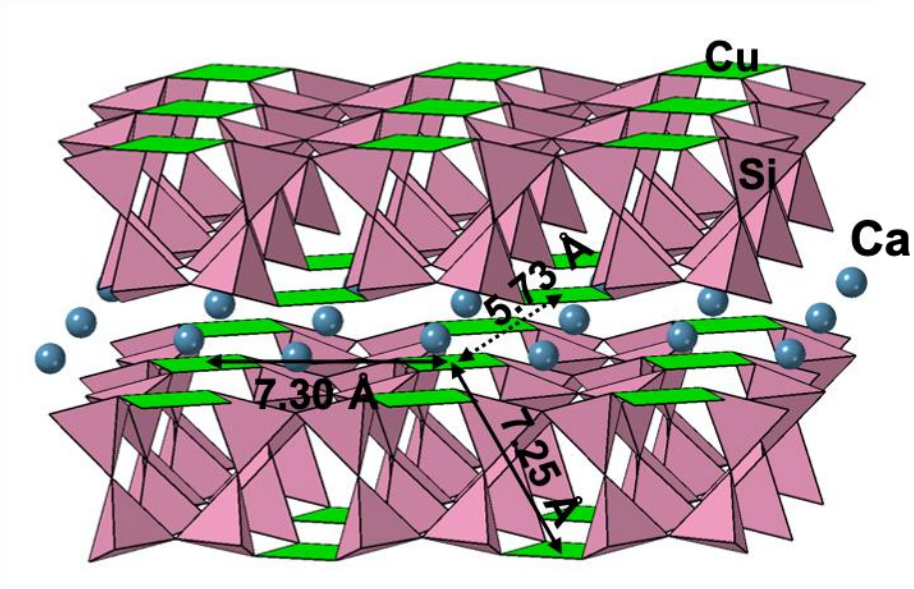


Figure 1. Structure of cuprorivaite $CaCuSi_4O_{10}$.

Cu^{2+} ions are inserted in the silicate layers in a plane-square coordination (D_{4h} site symmetry). Each of these ions carry an unpaired electron ($3d^9$ configuration) and owing to the fairly close proximity between neighboring Cu^{2+} ions, Heisenberg spin-spin exchange interactions can be expected. The purpose of this paper is to probe the magnetic interactions between Cu^{2+} ions in cuprorivaite by Electron Paramagnetic Resonance (EPR) and magnetic susceptibility measurements and the optical properties (absorption, emission and excitation) of this compound in the UV-visible range.

METHODS

Samples of cuprorivaite were prepared by solid state reaction starting from calcium carbonate $CaCO_3$, amorphous silica SiO_2 and copper oxide CuO and 3 w.\% of Na_2CO_3. The starting

materials were mixed and ground together then pressed into pellets under a unixial pressure of 4 tons/cm^2. The pellets were first sintered in air at 1000 °C for 5 hours. The resulting samples were then ground, pressed into new pellets and sintered again during 17 hours in air at 1000 °C.

X-ray diffraction (XRD) was performed on an X Panalytical X'Pert Pro diffractometer with the $K_{\alpha 1}$ ray of a copper anti-cathode λ=1.5406 Å). Raman spectra were acquired with a Invia Renishaw Raman microscope equipped with a 10 mW laser source emitting at 473 nm. XRD patterns and Raman spectroscopy showed that the samples were majoritarily made of cuprorivaite $CaCuSi_4O_{10}$ along with an amorphous phase and traces of Wollastonite $CaSiO_3$ and SiO_2 (see Supporting Information).

Electron Magnetic Resonance (EMR) spectra at X (9.392 GHz) and Q (34.22 GHz) bands were recorded with a Bruker Elexsys E500 equipped with an SHQE (X-band) or an ER5106QTW resonator (Q-band) and a Helium flow Oxford Instruments ESR900 cryostat for low temperature measurements. EPR at L (1.737 GHz) and S (4.8 GHz) bands was performed at room temperature with a home-made spectrometer equipped with a surface resonator. The simulations of the EPR spectra were performed with the Easyspin software, version 5.2.28.[17]

DC magnetic susceptibility measurements were performed using a conventional SQUID magnetometer MPMS-XL from Quantum Design working at a magnetic field up to 5 T and temperature down to 2 K. The measurements were done at 1 T and 5 T to ensure that no ferromagnetic contamination could have perturbed the quantitative extraction of the Curie-Weiss temperature and g-factor. The diamagnetism was corrected by the Pascal's constants 119×10^{-6} emu.mol^{-1}.

Optical absorption spectra were recorded at room temperature in diffuse relectance mode with a Cary 500 UV-Vis-NIR spectrometer. Near-Infrared (NIR) luminescence at room temperature was

recorded with an Ocean Optics HR2000+ spectrometer upon excitation at 633 nm with a He-Ne laser. Luminescence at room temperature in the UV-visible-near IR range was excited with a tunable YAG:Nd Eskpla pulsed laser and detected with a Jobin-Yvon HR250 monochromator and an ICCD camera.

RESULTS AND DISCUSSION

Exchange Interactions between Cu^{2+} ions in cuprorivaite. Figure 2 shows the EPR spectra of Cu^{2+} in a powder sample of cuprorivaite at L, S, X and Q bands and at room temperature. The X- and Q-band spectra reveal an axial symmetry for the g-matrix, with principal values g_x=g_y=2.060 and g_z=2.344. These g-values are typical of an unpaired electron localized in the $3d_{x^2-y^2}$ orbital of Cu^{2+}.[18] The g-matrix anisotropy is weakly resolved at S-band and no longer at all at L-band. The X-band spectrum is identical to those already reported for cuprorivaite.[19]

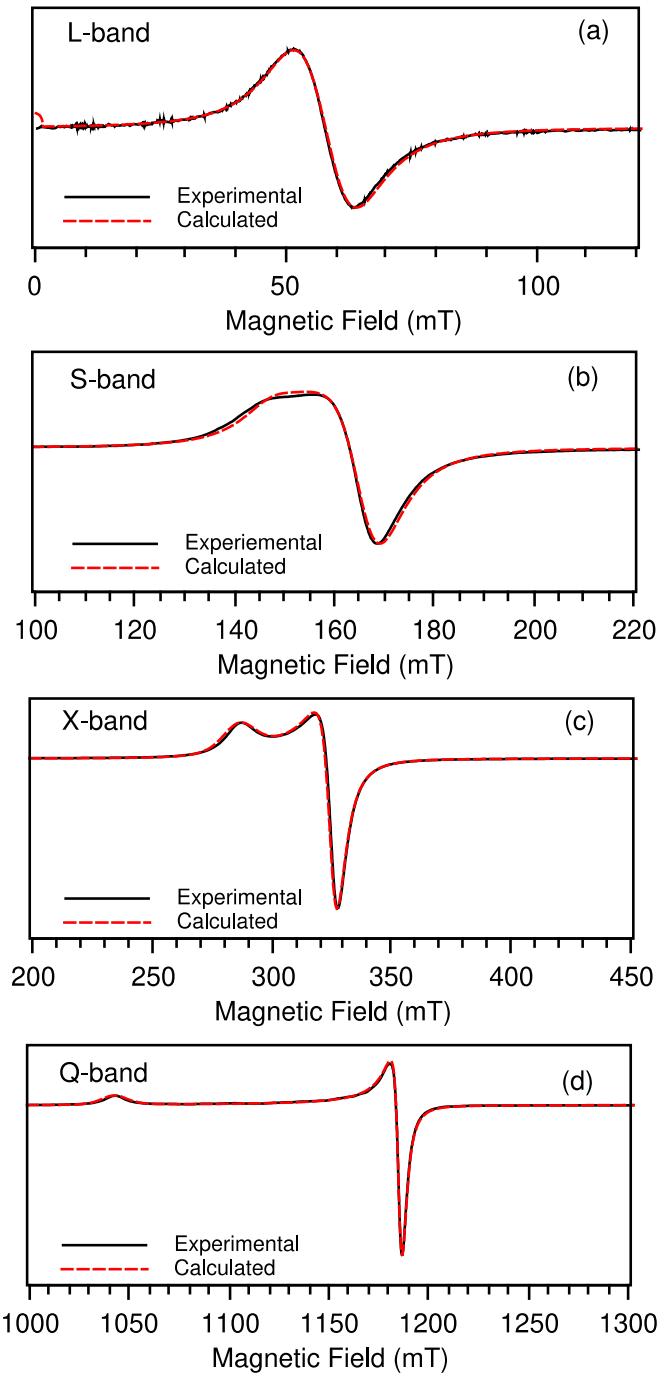


Figure 2. EPR spectra at room temperature of polycrystalline $CaCuSi_4O_{10}$. Microwave frequency (a) 1.737 GHz, (b) 4.8 GHz, (c) 9.392 GHz, (d) 34.22 GHz.

None of the spectra exhibit the hyperfine structure due to the coupling between the unpaired electron with the central ^{63}Cu or ^{65}Cu nucleus (nuclear spin I=3/2 for both isotopes), which is

usually observed with magnetically diluted Cu^{2+} impurities in solids. This suggests exchange interactions between Cu^{2+} ions in cuprorivaite strong enough to average out the hyperfine interaction. The exchange energy J can be determined from a measurement of the Curie-Weiss temperature θ of the spin system. These quantities are related by:[20]

$$\theta = \frac{zS(S+1)J}{3k} \quad (1)$$

with k the Boltzmann constant, z the number of nearest Cu^{2+} neighbors for a Cu^{2+} ion and S=1/2 the unpaired electron spin. The Curie-Weiss temperature θ is negative (positive) in case of antiferromagnetic (ferromagnetic) exchange interactions.

This temperature can be first determined from the temperature dependence of the EPR intensity I_{EPR}, which is proportional to the difference of populations between spin states, and in the paramagnetic domain given by:

$$I_{EPR} = \frac{A}{T-\theta} \quad (2)$$

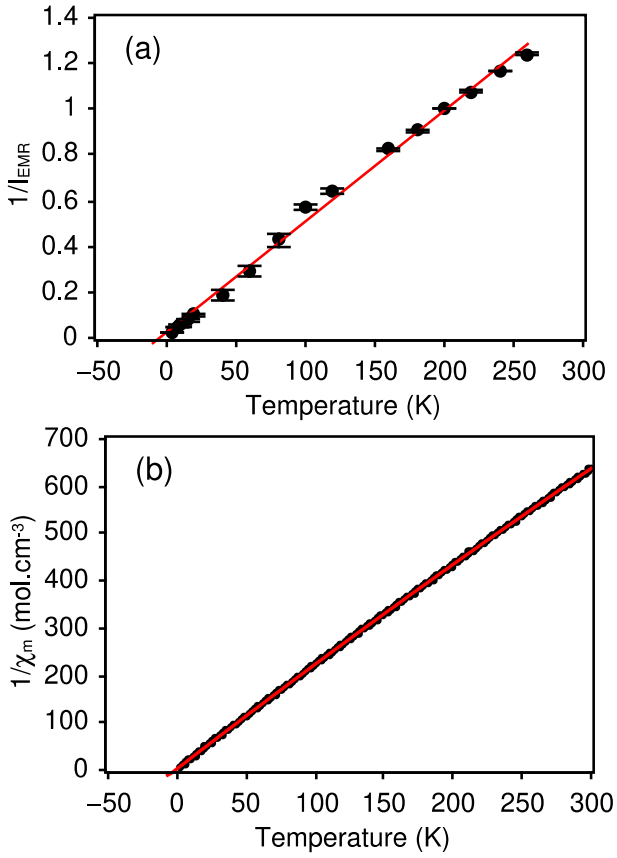


Figure 3. (a) Reciprocal of the intensity of the EPR signal at X-band of Cu^{2+} in $CaCuSi_4O_{10}$, (b) reciprocal of the molar static magnetic susceptibility of the sample, as a function of temperature. Full lines: values calculated from Eqs. 2 and 3, respectively.

Figure 3a shows the reciprocal of I_{EPR} recorded at X-band as a function of temperature. A straight line dependence is observed in agreement with Eq. 2, from which we get θ = -1.7 ± 0.8 K, indicating weak antiferromagnetic exchange interactions between Cu^{2+} ions. The Curie-Weiss temperature can also be determined from static magnetic susceptibility measurements. Figure 3b shows the reciprocal of the molar magnetic susceptibility χ_m as a function of temperature. The susceptibility was adjusted to:

$$\chi_m = \frac{C}{T-\theta} + \chi_{VV} \qquad (3)$$

where $C = g^2\beta^2 S(S+1)/3k$ is the Curie constant, with β the electron Bohr magneton and χ_{VV} is the temperature independent Van Vleck contribution. The simulation yielded θ = -1.9 ± 0.5 K, which confirms the antiferromagnetic nature of the exchange interactions, and C = 0.43 ± 0.01 $cm^3.mol^{-1}.K^{-1}$, g = 2.15 and $\chi_{VV} = 90 \times 10^{-6}$ $emu.mol^{-1}$ (common value for Cu^{2+} is 70×10^{-6} $emu.mol^{-1}$). Combining the results from EPR intensity and static magnetic susceptibility, we get an average value θ = -1.8 ± 0.9 K for the Curie-Weiss temperature of cuprorivaite. It must be noted that a similar value θ = -2 ± 3 K derived from magnetic susceptibility measurements was reported for the Han Blue $BaCuSi_4O_{10}$,[21] which is structurally analogous to cuprorivaite. In the structure, the M^{2+} ions (Ca^{2+} or Ba^{2+}) are located between $[CuSi_4O_{10}]^{2-}$ layers (Fig. 1) and the change of Ca^{2+} for Ba^{2+} widens the interlayer gap, with the interlayer Cu-Cu distance increasing from 5.73 Å to 6.08 Å. Therefore, the antiferromagnetic interactions must be mostly determined by coupling pathways within a single $[CuSi_4O_{10}]^{2-}$ layer and not between adjacent layers, despite the fact that the shortest Cu^{2+}-Cu^{2+} distance is between adjacent layers (Fig. 1). This is most certainly because the anion sublattice transmitting the super-exchange interactions is disrupted between layers. As a consequence, the number z of neighbors in Equation 1 should be the number of closest neighbors within a layer rather than the number of nearest neighbors in the whole lattice. Within a layer, a Cu^{2+} ion has z = 8 neighbors at 7.25-7.30 Å (Fig. 1). Equation 1 then yields the exchange energy J = -0.08 ± 0.04 meV. The corresponding exchange frequency ν_e can then be calculated from:[22]

$$\nu_e = 1.68\sqrt{S(S+1)}\frac{|J|}{h} \quad (4)$$

which gives ν_e = 27 ±14 GHz.

The exchange frequency can also be determined from the frequency dependence of the EPR linewidth. Indeed the contributions to the EPR line second moment from the non-secular parts of the electron-electron magnetic dipolar interactions decrease when the applied field (hence the

microwave frequency) increases, resulting in a field dependence of the EPR linewidth.[22, 23] The EPR spectra were simulated considering an unpaired electron spin S= ½ with axial g-factor anisotropy $(g_x = g_y = 2.060\,, g_z = 2.034)$ and an intrinsic peak-to-peak linewidth ΔB corresponding to a Lorentzian lineshape for the spin packets and, for a better match, a Gaussian distribution for the principal value g_z of the g-matrix with standard deviation $\sigma_{g_z} = 0.085$. Usually, the intrinsic linewidth ΔB in a low dimensional system is anisotropic and depends on the orientation of the applied magnetic field with respect to the crystal axes.[24] This angular dependence needs to be determined from a single crystal, which was not available. Therefore, a simply isotropic intrinsic peak-to-peak linewidth ΔB was considered in the simulations. The intrinsic peak-to-peak linewidths derived from the simulations of the EPR spectra at different microwave frequencies are shown in Figure 4.

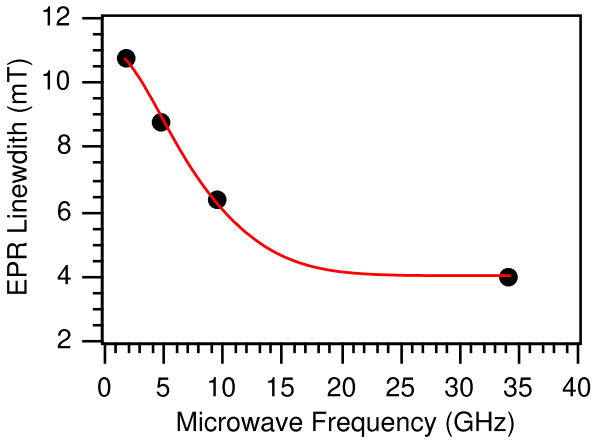


Figure 4. Intrinsic peak-to-peak linewidth of the EPR signal of Cu^{2+} in $CaCuSi_4O_{10}$ as a function of the microwave frequency. Full line: calculated values according to Eq. 5.

A fast decrease of the linewidth from 1.7 GHz (L-band) to 9.4 GHz (X-band) is observed followed by a slower decrease to 34 GHz (Q-band). In the exchange narrowing regime, the frequency dependence of the linewidth can be simulated with the following equation:[22, 23]

$$\Delta B = \Delta B_{dip}\left[1 + \frac{5}{3}e^{-0.5(\nu/\nu_e)^2} + \frac{2}{3}e^{-2(\nu/\nu_e)^2}\right] + \Delta B_{other} \quad (5)$$

where ν is the microwave frequency and ν_e the exchange frequency. In the above equation, the first term of the right-hand member is the electron dipolar contribution to the linewidth and the second term ΔB_{other} contains contributions from hyperfine interaction and possible anisotropic exchange interaction. The simulation yields $\Delta B_{dip} = 3.0 \pm 0.1$ mT, $\Delta B_{other} = 1.0 \pm 0.3$ mT and $\nu_e = 7.3 \pm 0.4$ GHz, a factor ≈ 4 lower than the ν_e value determined from the temperature dependence of the EMR intensity. It might be possible that the determination of the exchange frequency from the EPR intensity or the magnetic susceptibility is biased by the use of Eqs. (1) and (4), which are valid for a cubic lattice, while cuprorivaite has a non-cubic 2-dimensional structure. Anyhow, if we consider diluted complexes of Cu^{2+}, the largest hyperfine splitting is about 14 mT ≈ 0.4 GHz,[18] which is much smaller than the exchange frequency, whether determined from the EPR intensity and magnetic susceptibility or by the frequency dependence of the linewidth. This is the reason why the hyperfine interaction in Cu^{2+} ions in cuprorivaite is averaged out and not observed on the EPR spectra. The peak-to-peak linewidth at infinite frequency ΔB_{dip} is given by[22]

$$\Delta B_{dip} = \frac{2}{\sqrt{3}}\frac{B_{dip}^2}{B_e} \quad (6)$$

In the equation above B_e is the exchange field and B_{dip}^2 is the electron magnetic dipolar contribution to the inhomogeneous linewidth, given by[22]

$$B_{dip}^2 = 5.1\left(\frac{\mu_0}{4\pi} \times \frac{g\beta}{a^3}\right)^2 S(S+1) \quad (7)$$

with $a = 5.7 \times 10^{-10}$ m the shortest distance between Cu^{2+} ions, $S = 1/2$, and $g \approx 2.1$. From a rigorous perspective, Eq. 7 is valid for a cubic lattice of paramagnetic ions, which is not the case of Cu^{2+} ions in cuprorivaite. However and as far as orders of magnitude are concerned, the use of Eq. 7 should not introduce significant errors. The exchange field B_e is given by[22]

$$B_e = 1.68\frac{|J|}{g\beta}\sqrt{S(S+1)} \quad (8)$$

The use of Eqs. 6 to 8 with $\nu_e \approx 7$ GHz yields a theoretical value $\Delta B_{dip} \approx 2$ mT, which is smaller but close to the experimental value ≈ 3 mT. However, it must be considered that the experimental estimate is probably biased by the small amount of data, the approximate determination of the intrinsic EPR linewidth from powder-type spectral simulation and the fact that Eq. 7 only gives an approximate theoretical value of B_{dip}^2 for cuprorivaite. It should be noticed that using the value $\nu_e \approx 27$ GHz derived from the temperature dependence of the EPR intensity and of the magnetic susceptibility would lead to an even lower theoretical value for ΔB_{dip}. It appears that despite their high concentration in the host matrix, Cu^{2+} ions are weakly antiferromagnetically coupled, with an exchange interaction of the order of 10 GHz or 0.05 meV. This exchange interaction is also much too small to be observed on optical spectra, for the widths of the optical absorption or emission bands of Cu^{2+} in cuprorivaite are of the order of a few 0.1 eV. [5-8] Therefore, the optical properties of cuprorivaite can be discussed considering independent Cu^{2+} ions.

Optical Absorption of Cuprorivaite. Since only polycrystalline samples of cuprorivaite were available, optical absorption spectra were recorded in diffuse reflectance mode, whereby the reflexion coefficient R is measured and related to the absorption coefficient K by[25]

$$\frac{K}{S} = \frac{1-R^2}{2R} = f(R) \quad (9)$$

where S is the scattering coefficient. Figure 5 shows the variation of $f(R)^2$ as a function of the photon energy $h\nu$. In the visible range, the absorption bands at 1.58 eV, 2.00 eV and 2.26 eV corresponding to the optical transitions $^2B_{1g} \longrightarrow {}^2B_{2g}$, $^2B_{1g} \longrightarrow {}^2E_g$ and $^2B_{1g} \longrightarrow {}^2A_{1g}$, respectively, in a Cu^{2+} complex in D_{4h} symmetry[5, 8] can be easily identified. $^2B_{1g}$, $^2B_{2g}$, ^2E_g and

$^2A_{1g}$ states represent an unpaired electron in the $d_{x^2-y^2}$, d_{xy}, (d_{xz}, d_{yz}), and d_{z^2} orbitals, respectively. The absorption spectrum shows a minimum at about 2.8 eV, which explains the blue color of cuprorivaite. In the UV range two linear variations of $f(R)^2$ are shown by the straight lines in Fig. 5, the first one between *ca* 3 and 4.2 eV, the second one between *ca* 4.2 eV and 5 eV. These linear parts in a plot of $f(R)^n$ as a function of hν with $n = 2$ indicate direct allowed interband transitions,[20] with corresponding optical gaps $E_{g,1} \approx 2.8$ eV and $E_{g,2} \approx 4.2$ eV.

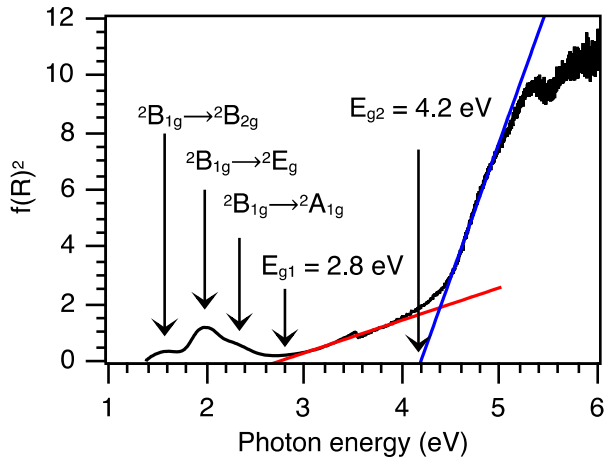


Figure 5. Optical absortion spectrum of polycrystalline $CaCuSi_4O_{10}$. Straight lines are linear extrapolations to determine the optical gaps $E_{g,1}$ and $E_{g,2}$.

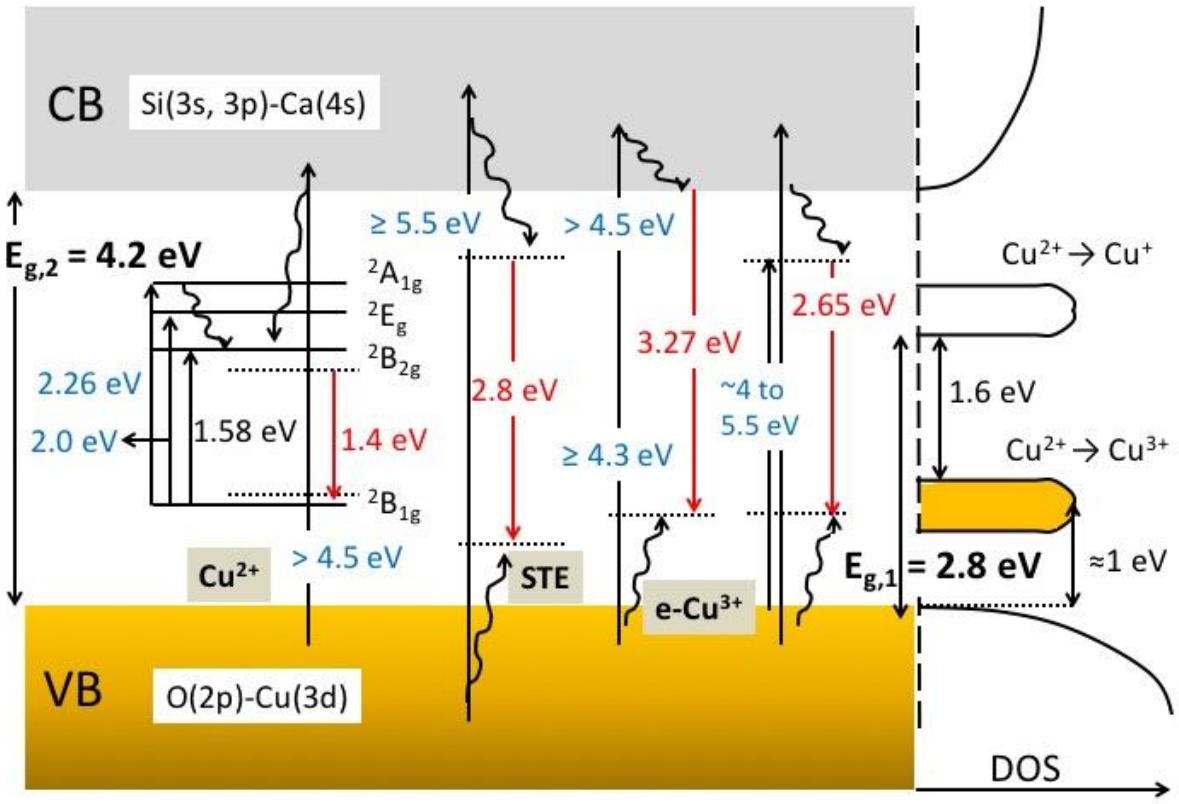


Figure 6. Simplified band structure of $CaCuSi_4O_{10}$ adapted from references 12 and 26, energy levels of Cu^{2+} in D_{4h} symmetry and optical transitions.

A schematic energy level diagram of Cu^{2+} in cuprorivaite is shown in the left part of Fig. 6, with the density of states (DOS) adapted from band structures calculations reported in references 12 and 26 represented in the right part of Fig. 6. From these calculations, $CaCuSi_4O_{10}$ turns to be a Mott-Hubbard insulator with a splitting of the upper Cu($3d$) levels into a filled $3d^9$ band and an empty $3d^{10}$ band approximately 1.6 eV above representing the energy of the corresponding Cu^+ levels. This 1.6 eV gap between the two Cu bands represent the energy required for the electron transfer $Cu^{2+} + Cu^{2+} \longrightarrow Cu^{3+} + Cu^{+}$. The narrow $3d^9$ band as well as the lower levels in the valence band (VB) show a significant Cu($3d$)-O($2p$) hybridization.[12, 26] A ≈ 2.8 eV gap exists between the VB (mostly made of O($2p$) orbitals) and the lowest narrow empty Cu^+ band (mostly made of Cu($3d$) orbitals), which could correspond to $E_{g,1}$. Thus, this gap corresponds to the ligand-

to-metal charge transfer (LMCT) transition. Also, a ≈ 4.2 eV gap exists between the VB and the conduction band CB, with mostly a Si(3*s*,3*p*)-Ca(4*s*) character (Fig. 6). This 4.2 eV gap matches the experimental value $E_{g,2}$ in Fig. 5.

Luminescence upon excitation in the UV range. The most studied luminescence from cuprorivaite is in the NIR range. A typical emission spectrum in this range upon excitation at 633 nm (1.96 eV) in the $^2B_{1g} \longrightarrow {}^2E_g$ absorption band of Cu^{2+} is shown in Fig. 7.

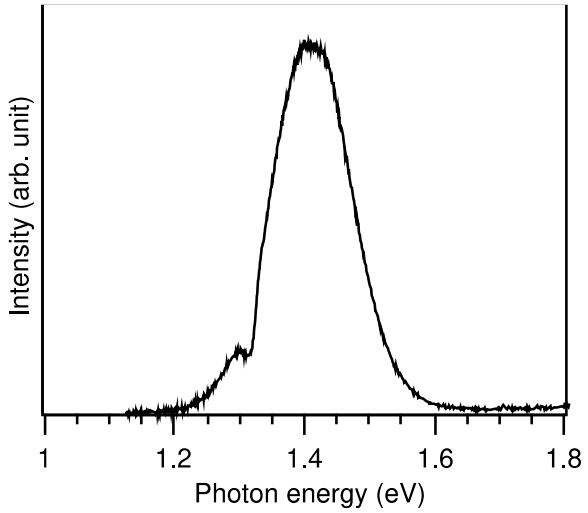


Figure 7. NIR photoluminescence of $CaCuSi_4O_{10}$ excited at 1.96eV.

The small dip at 1.3 eV in the flank of the emission band at ≈ 1.4 eV is most probably an artifact from the detector as it is not seen in other NIR emission spectra reported in literature except in Ref. 13 where a similar spectrometer as ours was used. The NIR emission at 1.4 eV corresponds to the $^2B_{2g} \longrightarrow {}^2B_{1g}$ transition with a ≈ 0.2 eV Stokes-shift. The excitation spectrum of the NIR emission monitored at 1.45 eV is shown in Fig. 8.

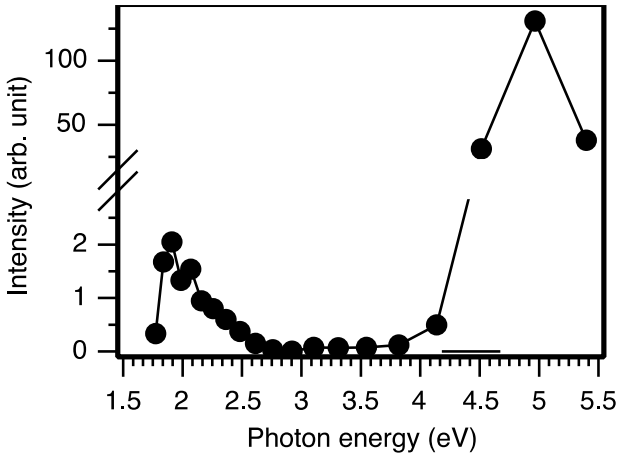


Figure 8. Excitation spectrum of the NIR luminescence at 1.45 eV in $CaCuSi_4O_{10}$.

This emission is excited by absorption from the intra-Cu^{2+} ion *d-d* transitions in the range 1.6-2.5 eV but it can also be much more efficiently excited by a factor about 60 in the UV range with an excitation peak at 5 eV corresponding to the VB-CB transition in Fig. 6.

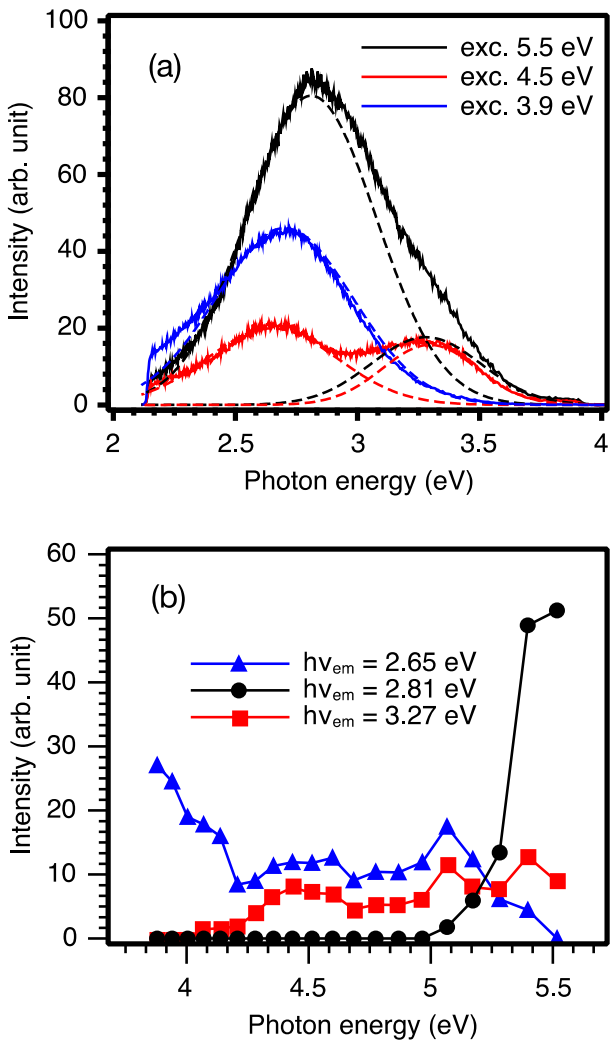


Figure 9. (a) UV-visible photoluminescence of $CaCuSi_4O_{10}$ upon UV excitation. Dashed lines are the calculated bands, simulated as Gaussian functions and contributing to the emission spectrum plotted with the same color. (b) Excitation spectra of the UV-visible emissions at 2.65 eV, 2.81 eV and 3.27 eV.

Other luminescence bands in the visible and UV range are also obtained by UV excitation (Fig. 9a). Three different emission bands can be observed, at 2.65 eV, 2.80 eV and 3.27 eV with relative intensities depending on the excitating photon energy, and with respective full width at half maximun (FWHM) 0.65 eV, 0.63 eV and 0.45-0.52 eV. The excitation spectra of these emissions

are shown in Fig. 9b. The emission at 2.65 eV is excited in the ≈ 3.5-5.5 eV range and the emission at 3.27 eV in the 4.2-5.5 eV range. The emission at 2.80 eV is excited at higher energy, at about 5.5 eV and possibly above.

The sample contains not only cuprorivaite $CaCuSi_4O_{10}$ as the majority phase but also traces of triclinic wollastonite $CaSiO_3$ and crystalline SiO_2 and an amorphous phase most probably a silicate one. The question the arises whether these emissions in the UV-visible range originate only from cuprorivaite or the other phases could also contribute. According to DFT-LDA band structure calculations, triclinic wollastonite has a band gap about 5.43 eV.[27] DFT-LDA generally underestimates gap values so that the true value should be even larger. Since the emissions at 2.65 eV, 2.80 eV and 3.27 eV are excited at photon energies closer to the gap value of $CaCuSi_4O_{10}$, it seems unlikely that these emissions arise from wollastonite. Similar emissions have also already been reported in SiO_2 either crystalline or amorphous. The emission at 2.8 eV is well-known in SiO_2[15,16,28-31] but excited above 8 eV in crystalline silica[29] and at 3.15 eV in amorphous silica,[32] thus at different energies from the excitation of the 2.8 eV emission in our sample. An emission at 3.27 eV is also known in crystalline SiO_2 and assigned to an electron recombination with a hole at a $[AlO_4]^0$ aluminum center formed after x-ray irradiation *i. e.* above the SiO_2 gap.[33] This luminescence needs thermal stimulation above room temperature. The conditions for observing this emission (presence of Al impurities, above SiO_2-gap excitation and thermal stimulation) makes unlikely its occurence from secondary SiO_2 phases in our sample with below SiO_2-gap excitation. An emission at 2.65 eV in amorphous SiO_2 has also been reported with an excitation maximum at 5 eV,[34] which does match the excitation spectrum of the 2.65 eV emission in the sample. Even if contributions of secondary $CaSiO_3$ or SiO_2 phases in our sample to the emissions at 2.65 eV, 2.80 eV and 3.27 eV cannot be fully excluded based on the present data, the fact that

their excitation energies match the optical gap of cuprorivaite and rather than the gap of $CaSiO_3$ or the excitation ranges of similar emissions in SiO_2 suggests that these emissions are most probably specific to cuprorivaite. In this compound, the emissions at 2.65 eV, 2.80 eV and 3.27 eV should originate from the recombinations of electron-hole pairs (excitons) either self-trapped or trapped by defects. Electrons may be trapped at oxygen vacancies, which manifest as three-fold coordinated silicon atoms.[35-37] These vacancies may be either native, for example for compensating Na^+ impurities in Ca^{2+} sites (since Na_2CO_3 was used in the synthesis), or may be created by high energy photon excitation.[28,38-40] In SiO_2, the hole may be trapped at oxygen sites in the form of peroxy defect, which may be native or created by oxygen displacement under high energy photon excitation.[16,28,41-47] Indeed, the well-known 2.7-2.87 eV emission in SiO_2 is commonly attributed to a self-trapped exciton (STE), [16,28,41-47] whereby an oxygen atom is displaced to a neighboring oxygen site, thus trapping the electron and the hole. As cuprorivaite is made of corner-sharing $[SiO_4]$ tetrahedra (Fig. 1) these types of oxygen defects are likely to exist also in this material. Therefore, the luminescence band at 2.8 eV in cuprorivaite excited at energy above 5.5 eV (Fig. 9b) may be interpreted as a self-trapped exciton (STE) emission, involving similar trapping defects as in SiO_2. In addition, holes formed in cuprorivaite may also be trapped at Cu^{2+} sites, giving Cu^{3+} defects. The emissions at 3.27 eV, 2.65 eV and 1.4 eV excited in the UV may be then attributed to excitons trapped at Cu site. The electron comes from either the CB edge (emission at 3.27 eV) or from an electron trapped at a neighboring defect (emission at 2.65 eV) as suggested by the excitation energy below the $E_{g,2} = 4.2$ eV gap. The NIR emission at 1.4 eV excited in the UV would result from the trapping of an exciton at a copper site yielding an excited Cu^{2+}, which then emits an NIR photon through the $^2B_{2g} \longrightarrow {}^2B_{1g}$ transition.

Figure 10 shows the photoluminescence decay at room temperature of the emissions at 3.27, 2.80 and 2.65 eV. These emissions exhibit nearly exponential decays with mean lifetimes $\tau = 8$ µs, $\tau = 34$ µs, and $\tau = 31$ µs, respectively. These lifetimes are typical of exciton emission lifetimes in quartz and strontium titanate for example,[28, 30, 31, 48] and are related to forbidden triplet-singlet exciton recombinations.

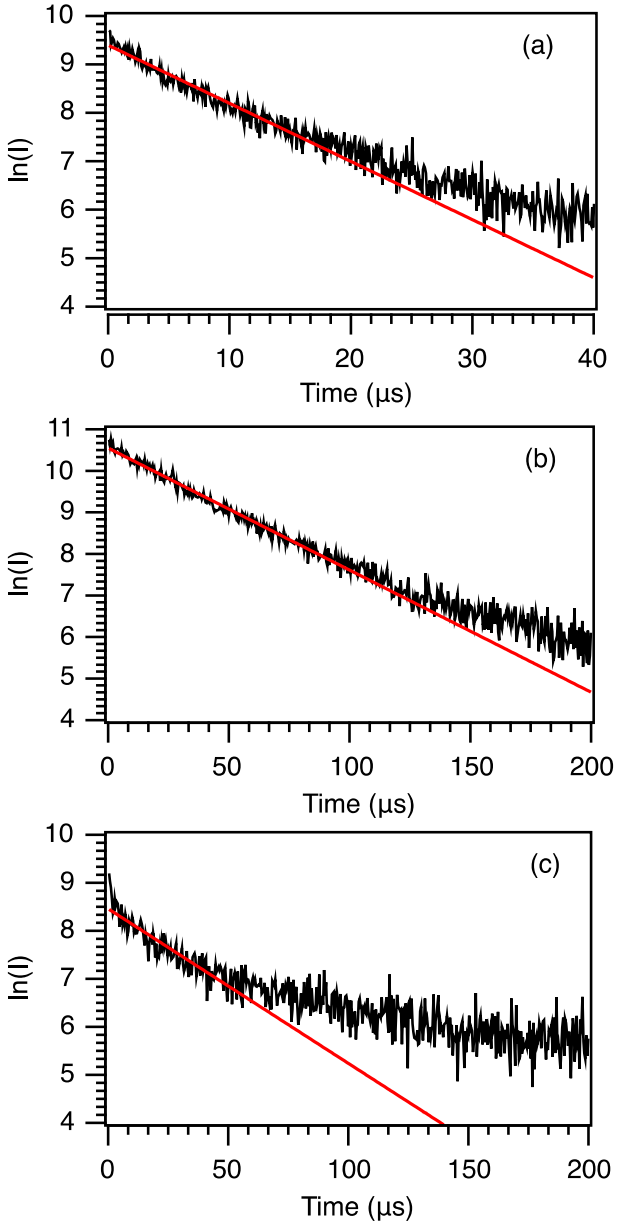


Figure 10. Time decay of the intensities I of the photoluminescence at (a) 3.3 eV, (b) 2.8 eV and (c) 2.6 eV. Straight lines: simulations with a decay law $\ln(I) = A - t/\tau$.

CONCLUSION

The magnetic and optical properties of cuprorivaite $CaCuSi_4O_{10}$ were investigated. Weak Heisenberg antiferromagnetic interactions between Cu^{2+} ions were revealed, which are responsible for an exchange narrowing of the hyperfine interaction between the unpaired electron on Cu^{2+} and the ^{63}Cu and ^{65}Cu nuclei. The high intensity of the EPR signal, even at low microwave frequency, raises the potential for using portable EPR spectrometers[49,50] for detecting cuprorivaite and its alteration products in archeological objects. It was shown that the well-known NIR luminescence of Cu^{2+} ions could be much more efficiently excited through the gap in the UV range, at 5 eV, than in the intra-ion *d-d* absorption bands. This raises a potential interest for the detection of traces of cuprorivaite in archeological context. Three luminescence bands in the UV-visible range could also be observed upon excitation above 4 eV by through-gap transitions. These UV-visible emissions are tentatively interpreted as arising from cuprorivaite and proposed to result from triplet-singlet recombinations of self-trapped excitons and trapped excitons. Further investigations are however needed with varying elaboration conditions, additives, precursor purities to ascertain the above interpretation, to determine the potential influence of native defects on the UV-visible luminescence, and to determine the potential contribution of secondary phases. This would then make possible the use of UV-visible photoluminescence as a marker of the origin and the elaboration process of archeological samples of Egyptian blue pigments made of cuprorivaite.

ASSOCIATED CONTENT

Supporting Information.

Photos, X-ray diffraction pattern and Raman spectrum of the sample

File: Cuprorivaite_magnetic_optical_properties-Supplementary_information.pdf

AUTHOR CONTRIBUTIONS

Laurent Binet analyzed and interpreted the results and wrote the paper. Juliette Lizion performed the material synthesis and structural characterization, the X and Q-band EMR, the optical measurements and analyzed the corresponding data. Sylvain Bertaina performed the L and S-band EMR and magnetic susceptibility measurements and analyzed the corresponding data. Didier Gourier contributed to the interpretation of the results and the writing of the paper. The manuscript was written through contributions of all authors. All authors have given approval to the final version of the manuscript.

ACKNOWLEDGMENT

This work was supported by Agence Nationale pour la Recherche (grant number ANR-17-CE29-0002-01).

REFERENCES

(1) Pagès-Camagna, S.; Colinart, S.; Coupry, C. Fabrication processes of archaeological Egyptian blue and green pigments enlightened by Raman microscopy and scanning electron microscopy. *J. Raman Spectros.* **1999**, *30*, 313–317.

(2) Pagès-Camagna, S.; Reiche, I.; Brouder, C.; Cabaret, D.; Rossano, S.; Kanngießer, B.; Erko, A. New insights into the colour origin of archaeological Egyptian blue and green by XAFS at the Cu K-edge. *X-Ray Spectrom.* **2006**, *35*, 141–145.

(3) Jaksch, H.; Seipel, W.; Weiner, K. L.; Goresy, A. E. Egyptian blue - Cuprorivaite a window to ancient Egyptian technology. *Naturwissenschaften* **1983**, *70*, 525–535.

(4) Berke, H. The invention of blue and purple pigments in ancient times. *Chem. Soc. Rev.* **2007**, *36*, 15–30.

(5) Ford, R. J.; Hitchman, M. A. Single crystal electronic and EPR spectra of $CaCuSi_4O_{10}$, a synthetic silicate containing copper (II) in a four-coordinate, planar ligand environment. *Inorg. Chim. Acta* **1979**, *33*, L167–L170.

(6) García-Fernández, P.; Moreno, M.; Aramburu, J. A. Origin of the exotic blue color of copper-containing historical pigments. *Inorg. Chem.* **2014**, *54*, 192–199.

(7) Accorsi, G.; Verri, G.; Bolognesi, M.; Armaroli, N.; Clementi, C.; Miliani, C.; Romani, A. The exceptional near-infrared luminescence properties of cuprorivaite (Egyptian blue). *Chem. Commun.* **2009**, *36*, 3392-3394.

(8) Pozza, G.; Ajo, D.; Chiari, G.; De Zuane, F.; Favaro, M. Photoluminescence of the inorganic pigments Egyptian blue, Han blue and Han purple. *J. Cult. Heritage* **2000**, *1*, 393–398.

(9) Kendrick, E.; Kirk, C. J.; Dann, S. E. Structure and colour properties in the Egyptian blue family, $M_{1-x}M_xCuSi_4O_{10}$, as a function of M, M where M, M = Ca, Sr and Ba. *Dyes Pigm.* **2007**, 73, 13–18.

(10) Borisov, S. M.; Würth, C.; Resch-Genger, U.; Klimant, I. New life of ancient pigments: Application in high-performance optical sensing materials. *Anal. Chem.* **2013**, *85*, 9371–9377.

(11) Errington, B.; Lawson, G.; Lewis, S.W.; Smith, G. D. Micronised Egyptian blue pigment: A novel near-infrared luminescent fingerprint dusting powder. *Dyes Pigm.* **2016**, *132*, 310–315.

(12) Li, Y. -J.; Ye, S.; Wang, C. -H.; Wang, X. -M.; Zhang, Q. -Y. Temperature-dependent near-infrared emission of highly concentrated Cu^{2+} in $CaCuSi_4O_{10}$ phosphor. *J. Mat. Chem. C* **2014**, *2*, 10395–1040.

(13) Berdahl, P.; Boocock, S. K.; Chan, G. C. -Y.; Chen, S. S.; Levinson, R. M., and Zalich, M. A., "High quantum yield of the Egyptian blue family of infrared phosphors ($MCuSi_4O_{10}$). *J. Appl. Phys.* **2018**, *123*, 193103.

(14) Schvoerer, M.; Delavergne, M. C.; Chapoulie, R. The thermoluminescence (TL) of Egyptian blue. *Int. J. Radiat. Appl. Instrum. Part D*. **1988**, *14*, 321–327.

(15) Itoh, C.; Tanimura, K.; Itoh, N. Optical studies of self-trapped excitons in SiO_2. *J. Phys. C: Solid State Phys.* **1988**, *21*, 4693–4702.

(16) Trukhin, A. N. Excitons in SiO_2: a review. *J. Non-Cryst. Solids* **1992**, *149*, 32–45.

(17) Stoll, S.; Schweiger, A.; EasySpin, a comprehensive software package for spectral simulation and analysis in EPR. *J. Magn. Reson.* **2006**, *178*, 42–55.

(18) Abragam, A.; Bleaney, B. *Electron Paramagnetic Resonance of Transition Ions*, Clarendon Press: Oxford, UK, 1970; p. 459.

(19) Orsega, E. F.; Agnoli, F.; Mazzocchin, G. A. An EPR study on ancient and newly synthesised Egyptian blue. *Talanta* **2006**, *68*, 831–835.

(20) Madelung, O. *Introduction to Solid-State Theory*, Springer-Verlag, 1981.

(21) Masunaga, S. H.; Rebello, A.; Schye, A. T.; Prasai, N.; Neumeier, J. J.; Cohn, J. L. Heat capacity, thermal expansion and heat transport in the Han blue ($BaCuSi_4O_{10}$): Observation of structural phase transitions. *J. Phys. Chem. Solids* **2015**, *85*, 69–74.

(22) Anderson, P. W.; Weiss, P. R. Exchange narrowing in paramagnetic resonance. *Rev. Mod. Phys.* **1953**, *25*, 269–276.

(23) Kubo, R.; Tomita, K., A general theory of magnetic resonance absorption. *J. Phys. Soc. Japan* **1954**, *9*, 888–919.

(24) Bencini, A.; Gatteschi, D. *EPR of Exchange Coupled Sytems*, Springer-Verlag, 1990; p. 155.

(25) Kubelka, P. New contributions to the optics of intensely light-scattering materials. Part I. *J. Opt. Soc. Am.* **1948**, *38*, 448–457.

(26) Chen, Y.; Kan, M.; Sun, Q.; Jena, P. Structure and properties of Egyptian blue monolayer family: $XCuSi_4O_{10}$ (X = Ca, Sr, and Ba). *J. Phys. Chem. Lett.* **2016**, *7*, 399–405.

(27) Henriques, J.M.; Caetano, E.W.S.; Freir, V.N.; da Cost, J.A.P.; Albuquerque, E.L. Structural and electronic properties of CaSiO3 triclinic. *Chem. Phys. Lett.* **2006**, *427*, 113–116

(28) Tanimura, K.; Tanaka, T.; Itoh, N. Creation of quasistable lattice defects by electronic excitation in SiO_2. *Phys. Rev. Lett.* **1983**, *51*, 423–426.

(29) Itoh, C.; Tanimura, K.; Itoh, N.; Itoh, M. Threshold energy for photogeneration of self-trapped excitons in SiO_2. *Phys. Rev. B* **1989**, *39*, 11183–11186.

(30) Skuja, L. N.; Entzian, W. Cathodoluminescence of intrinsic defects in glassy SiO_2, thermal SiO_2 films, and -quartz. *Phys. Status Solidi (a)* **1986**, *96*, 191–198.

(31) Trukhin, A. N. Temperature dependence of luminescence decay kinetics of self-trapped excitons, germanium and aluminium centres in crystalline quartz. *Phys. Status Solidi (b)* **1987**, *143*, K83–K88.

(32) Skuja L. Direct singlet-to-triplet optical absorption and luminescence excitation band of the twofold-coordinated silicon center in oxygen-deficient glassy SiO_2. *J. Non-Cryst. Solids* **1994**, *167*, 229-238

(33) Martini, M.; Paleari, A.; Spinolo, G.; A. Vedda Role of $[A1O_4]^0$ centers in the 380-nm thermoluminescence of quartz. *Phys. Rev. B* **1995**, *52*, 138-142

(34) Skuja, L.N.; Streletsky, A.N. and Pakovich, A.B. A new intrinsic defect in amorphous SiO_2: Twofold coordinated silicon. *Solid State Commun.* **1984**, *50*, 1069-1072

(35) Feigl, F. J.; Fowler, W.; Yip, K. L. Oxygen vacancy model for the E_1' in SiO_2. *Solid State Commun.* **1974**, *14*, 225-229.

(36) Rudra, J. K.; Fowler, W. B. Oxygen vacancy and the E' center in crystalline SiO_2. *Phys. Rev. B* **1987**, *35*, 8283–8230.

(37) Yip, K. L.; Fowler, W. B. Electronic structure of E_1' centers in SiO_2. *Phys. Rev. B* **1975**, *11*, 2327-2338.

(38) Tsai, T. E.; Griscom, D. L.; Friebele, E. J. Mechanism of intrinsic Si E'-center photogeneration in high-purity silica. *Phys. Rev. Lett.* **1988**, *61*, 444-446.

(39) Tsai, T. E.; Griscom, D. L. Experimental evidence for excitonic mechanism of defect generation in high-purity silica. *Phys. Rev. Lett.* **1991**, *67*, 2517-2520.

(40) Saeta, P. N.; Greene, B. I. Primary relaxation process at the band edge of SiO_2. *Phys. Rev. Lett.* **1993**, *70*, 3588-359.

(41) Shluger, A.; Stefanovich, E. Models of the self-trapped exciton and nearest-neighbor defect pair in SiO_2. *Phys. Rev. B* **1990**, *42*, 9664–9673.

(42) Fisher, A. J.; Hayes, W.; Stoneham, A. M. Structure of the self-trapped exciton in quartz. *Phys. Rev. Lett.* **1990**, *64*, 2667–2670.

(43) Ramo, D. M.; Sushko, P. V.; Shluger, A. L. Models of triplet self-trapped excitons in SiO_2, HfO_2, and $HfSiO_4$. *Phys. Rev. B* **2012**, *85*, 024120.

(44) Azzoni, C. B.; Meinardi, F.; Paleari, A. Trapped-hole centers in neutron-irradiated synthetic quartz. *Phys. Rev. B* **1994**, *49*, 9182–9185.

(45) Ismail-Beigi, S.; Louie, S. G. Self-trapped excitons in silicon dioxide: Mechanism and properties. *Phys. Rev. Lett.* **2005**, *95*, 156401.

(46) Griscom, D. L. Trapped-electron centers in pure and doped glassy silica: A review and synthesis. *J. Non-Cryst. Solids* **2011**, *357*, 1945–1962.

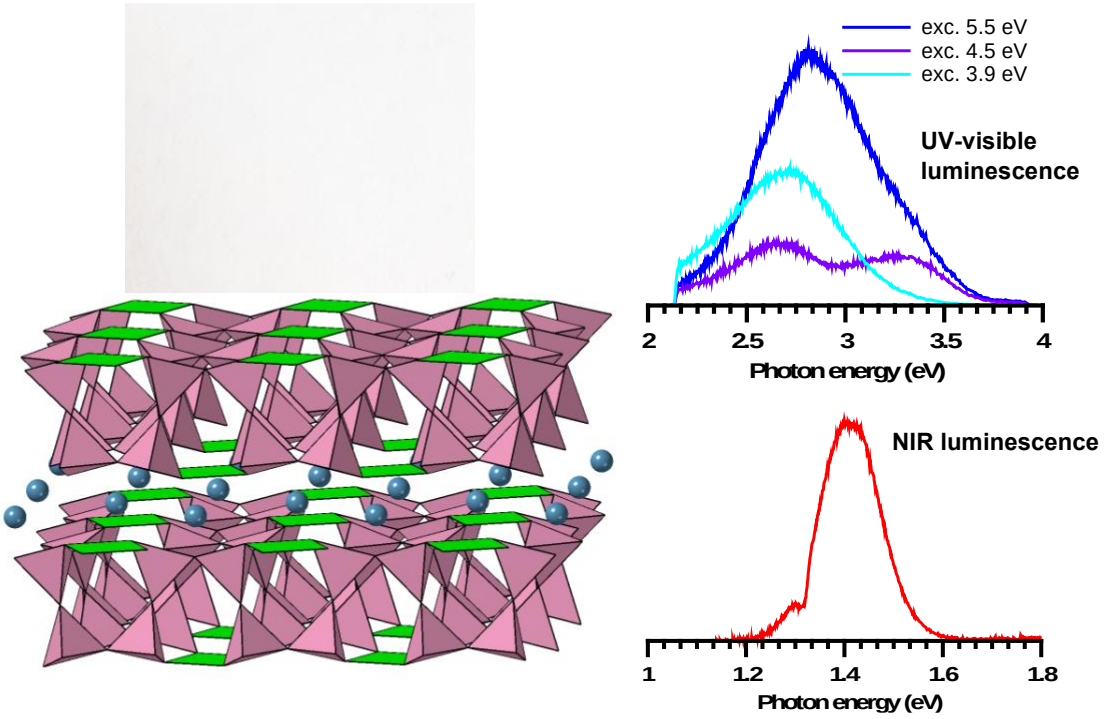
(47) Paleari, A.; Meinardi, F.; Brovelli, S.; Lorenzi, R. Competition between green self-trapped-exciton and red non-bridging-oxygen emissions in SiO_2 under interband excitation. *Commun. Phys.* **2018**, *1*, 1–12.

(48) Crespillo, M. L., Graham, J. T.; Agulló-López, F.; Zhang, Y.; Weber, W. J. Recent advances on carrier and exciton self-trapping in strontium titanate: Understanding the luminescence emissions. *Crystals* **2019**, *9*, 95-111.

(49) Switala, L. E.; Black, B. E.; Mercovich, C.; Seshadri, A.; Hornak, J. An electron paramagnetic resonance mobile universal surface explorer. *J. Magn. Reson.* **2017**, *285*, 18–25.

(50) Javier, S.; Hornak, J. A nondestructive method of identifying pigments on canvas using low frequency electron paramagnetic resonance spectroscopy. *J. Am. Inst. Conserv.* **2018**, *57*, 73–82.

TOC graphic


exc. 5.5 eV
exc. 4.5 eV
exc. 3.9 eV
UV-visible
luminescence
2
2.5
3
3.5
4
Photon energy (eV)
NIR luminescence
1
1.2
1.4
1.6
1.8
Photon energy (eV)

Magnetic And New Optical Properties In The UV-Visible Range Of The Egyptian Blue Pigment Cuprorivaite $CaCuSi_4O_{10}$

Laurent Binet [a], Juliette Lizion [a #], Sylvain Bertaina [b] and Didier Gourier [a]*

[a] Chimie-ParisTech, PSL University, CNRS, Institut de Recherche de Chimie-Paris, 11 rue Pierre et Marie Curie, 75005 Paris, France

[b] Aix-Marseille Université, CNRS, Institut Matériaux, Microélectronique et Nanosciences de Provence, Avenue Escadrille Normandie-Niemen, 13397 Marseille cedex 20, France

** Email: laurent.binet@chimieparistech.psl.eu*

Present Address

 # Université de Montpellier, Institut Charles Gerhardt Montpellier, CNRS-UM-ENSCM, Place Eugène Bataillon, 34095 Montpellier cedex 5, France

Supporting Information

Table of content

1. Sample photo
2. X-ray diffraction
3. Raman spectroscopy

1. Sample photo

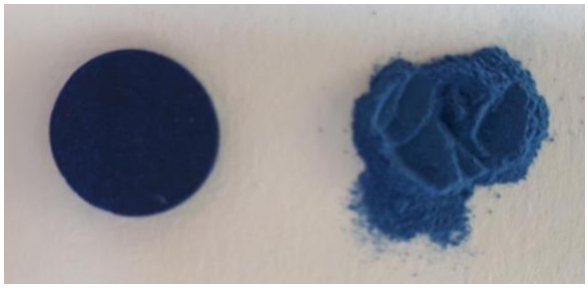


Figure S1: Photo of an as prepared pellet and of the powder from a ground pellet

2. X-ray diffraction

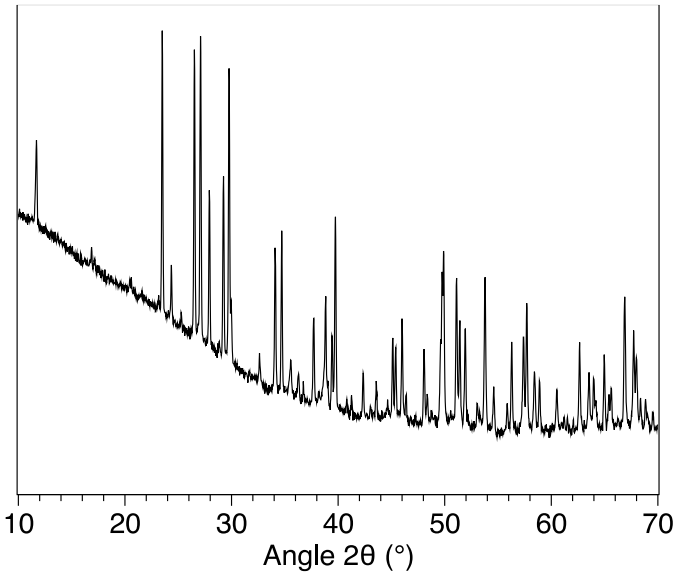


Figure S2: X-Ray Diffraction pattern of the Egyptian Blue sample (Cu $K_{\alpha 1}$, λ=1.5406 Å), showing the crystalline phases and the background due to amorphous phases.

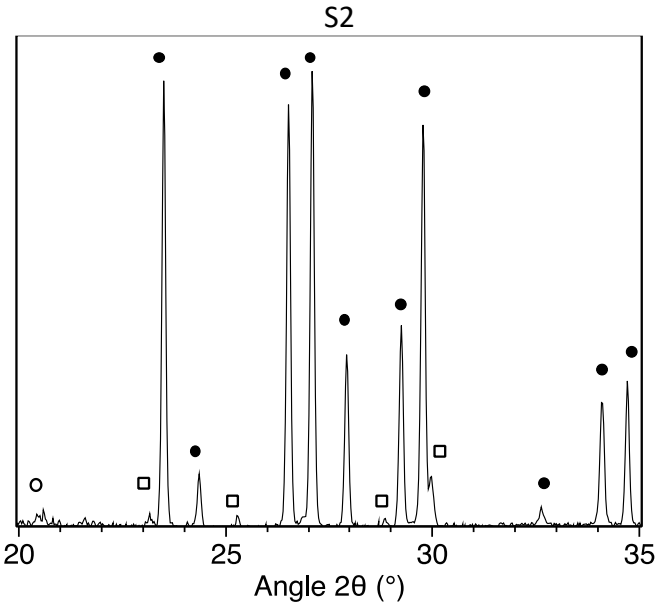


Figure S3: Expended view of the X-ray diffraction pattern (Cu $K_{\alpha 1}$, λ=1.5406 Å) of the Egyptian blue sample after background removal. Filled circles: cuprorivaite $CaCuSi_4O_{10}$ (ICDD 04-009-5400); squares: triclinic wollastonite $CaSiO_3$ (ICDD 04-011-2265); open circle: SiO_2 (ICDD 01-082-1553)

3. Raman spectroscopy

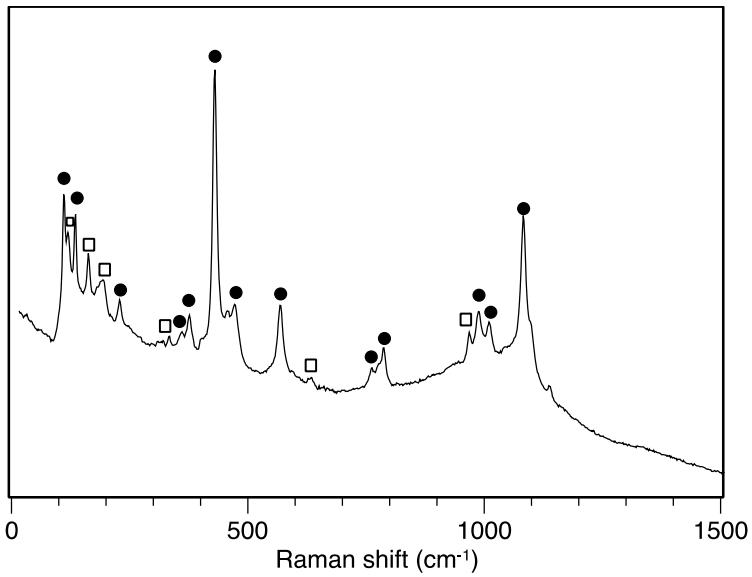


Figure S4: Raman spectrum of the Egyptian blue sample. Circles: cuprorivaite $CaCuSi_4O_{10}$, squares: wollastonite $CaSiO_3$. AssignmentS from S. Pagès-Camagna *et al.*, Journal of Raman Spectroscopy 30, 313-317 (1999). The broad band at 1000-1100 cm^{-1} below the sharp lines indicates the presence of an amorphous silica phase (P. McMillan, American Mineralogist 69, 622-444 (1984))

S3